Temperature-Induced Deformation in a Mechanical System

P. Poonyapak* M.J.D. Hayes† J.M.J. McDill‡
Mechanical and Aerospace Engineering,
Carleton University,
Ottawa, ON., Canada

Abstract—*Eliminating the warm-up cycle times needed when an industrial robot is not operated in a thermally stable condition is desirable. A benchmark investigation of the temperature-induced deformation of a driven single aluminum (6061-T6) link is presented. A thermal imaging camera records the time-dependent temperature history of the link. Two experimental cases are reported. The first involves stationary heating of the link. An analytical approach to estimating the distortion of the link allows comparison of the temperature-induced deformation to the recorded drift. In the second case, motion is introduced and the recorded drift is compared to the temperature-induced deformation predicted by a transient finite element analysis (FEA). Incorporating a simple compensation algorithm in the robot controller is presented as a step towards reduction of warm-up cycle times.*

Keywords: Temperature-induced deformation; industrial robot; warm-up time; transient thermal-mechanical FEA

I. Introduction

The long-term goal of this work is to eliminate the warm-up cycle times needed when an industrial robot is not operated in a thermally stable condition. The thermal instability is induced by losses in the robot motors and gearboxes, and typically requires two hours of continuous motion through the reachable workspace at 100% motor speed in order to reach steady state [1]. During the warm-up, the workcell has zero productivity, substantially increasing production costs. Moreover, if the robot workcell must go offline, the resulting cool-down will require additional warm-up cycles.

To the best of the authors' knowledge, with the exception of the investigation of temperature-induced errors in CNC machine tools [2], there exists little archival literature studying the contribution of temperature-induced deformation in the robot kinematic geometry during warm-up. The elimination of the temperature-induced deformation will enhance the repeatability of the robot workcell. There is a very broad spectrum of conceptual approaches to the robot repeatability; e.g., [3], [4], [5], [6], [7], [8], [9], [10], [11], [12], [13], [14].

To investigate temperature-induced deformation relating to robot geometry, the behaviour of a simplified robot mechanical system comprising one motor and one link is considered. The link, a 6061 Al alloy in the T6 heat-treated condition, is attached to the shaft of a servo motor in a manner similar to those used in small payload industrial robots. The motion of the apparatus is controlled by the wrist motion (sixth axis) of a Thermo CRS A465 robot. Heat is transferred to the link causing temperature-induced deformation. To reduce the complexity of the experiment, the link used is slender, so that the longitudinal deformation dominates.

The experiment considers two cases: a stationary link and a moving link. The experimental data include temperature distribution and dimensional changes of the slender link over a period of several hours. Measurements obtained from the experiment are compared to the results from their corresponding analytical (theoretical) and numerical (FEA) analyses.

*E-mail: ppoon@mae.carleton.ca
†E-mail: jhayes@mae.carleton.ca
‡E-mail: mmcdill@mae.carleton.ca

II. Description of the experimental apparatus

The experimental setup is shown in Figure 1. It incorporates the simplified robot mechanical system and the optical measurement system.

A laser diode, tuned to be nearly invisible, mounted to the distal end of the link, points directly onto the CCD chip of a digital camera; i.e., no lens.

A. Simplified robot mechanical system

The link has a length-to-width ratio of 10 ensuring that the longitudinal deformation dominates the effects caused by an increase in temperature. The link is 13 in (33.02 cm) long, 1 in (2.54 cm) wide and 0.25 in (0.64 cm) thick. It has a hole at each end to accommodate the driving shaft and a laser diode respectively. The centre of the motor shaft hole is located at 1 in (2.54 cm) from the proximal end of the shaft. The centre of the hole for the laser diode is located 0.52 in (1.32 cm) away from the distal end of the link.

The link is painted flat black, emissivity $\simeq 0.95$ [15], to reduce infrared and visible spectrum reflections which induce uncertainty for temperature readings in the experiment.

As illustrated in Figure 1, the link is attached to an output shaft of a servo motor. A Thermo CRS A465 robot system consisting of a 6-axis A465 robot arm, and a C500C con-

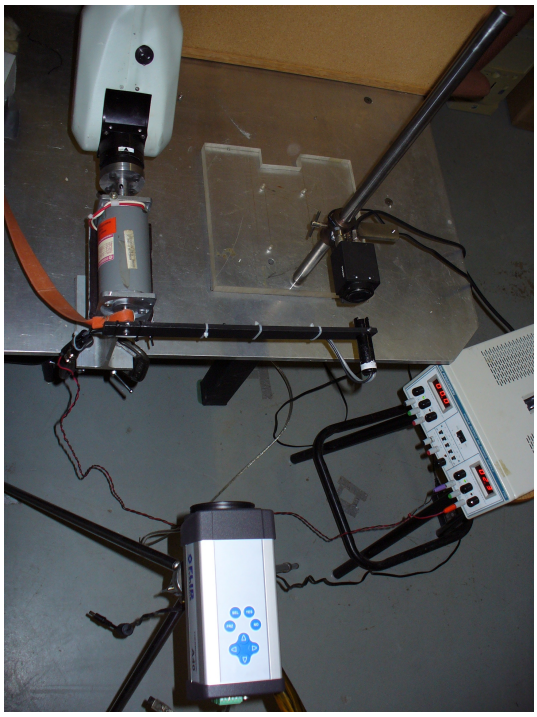

Fig. 1. Experimental apparatus

troller, can be used to impart motion to the link in a reciprocating 180° arc.

While the motion control is provided through the A465 robot, both stationary and moving cases are examined. Therefore, the shaft is thermally insulated from the robot wrist and a silicone heating pad is used to provide consistent local heating. The heating pad is wrapped around the output shaft between the motor case and the 6061 Al link. The temperature was increased from approximately 22°C to approximately 42°C in the moving case and from approximately 22°C to approximately 36°C in the stationary case. The end temperature in the stationary case is slightly lower than in the moving case due to the difficulties experienced in maintaining the temperature of the heating pad. Time did not permit a repeat of the moving case at the lower temperature.

A.1 Optical measurement system

Temperature measurements are obtained using a FLIR A40M infrared camera. The detector is a Focal Plane Array (FPA), uncooled microbolometer with spatial resolution of 1.3 mrad and thermal sensitivity of 0.08°C at 30°C. The temperature range used is -40°C to 120°C, with an accuracy of ±2°C full scale.

Longitudinal deformation is measured by tracking the drift of a laser diode spot across a CCIR standard Pulnix TM-6CN camera CCD chip. Image distortion was attenuated by pointing the laser directly on the CCD chip. The cell size is 8.6 (H) x 8.3 (V) μm, and its resolution is 752 (H) x 582 (V) pixels. The camera is adjusted to manual gain control in field mode. The following settings are used: gamma = 0.45; blacklevel = 0.1 mV; whitelevel = 0.7 mV; electronic shutter speed = 1/10000 s. The framegrabber is a National Instrument PCI-1409 monochrome. The laser diode is made by StockerYale and has a wavelength of 635 nm. It is tuned to be almost invisible to enhance the accuracy of the laser spot centroid extraction algorithm. The algorithm extracts the geometric centroid of the laser spot by summing the pixel moments in two orthogonal directions [16].

The CCD camera is placed so that the laser diode points straight onto the CCD chip when the link is in its home position: i.e., the link is parallel to the horizontal plane and stays on the righthand side of the motor when viewed from the front. The infrared camera is located to obtain the front view of the link when in the home position, as shown in Figure 1. Combined, these two cameras provide a contactless measurement system.

III. Procedure

The experiment considers two cases: stationary and moving. The stationary case maps the temperature-induced deformation to the temperature changes, and eliminates the effects of motion, although some free convection occurs. The convection coefficient h has been estimated to be $4.55\frac{W}{m^2\ K}$ [18].

In the moving case, motion-induced mechanical effects as well as some forced convection are introduced, where h has been estimated to be $7.75\frac{W}{m^2\ K}$ [18]. Results from these cases will be compared with their corresponding analytical and numerical models.

A. Stationary case

In the stationary case, the 6061 Al link is permanently set in the home position. Heat is applied through the heating pad. The temperature increases from 22°C to 36°C over several minutes.

The CCD camera captures a single image of the laser spot every 2 minutes for 1 hour (31 images). Similarly, the infrared camera records 31 images of the temperature distribution.

B. Moving case

In the moving case, the link rotates continuously through 180° between the home position and a goal position; i.e., windshield wiper motion, for one hour. At 30 second intervals, the link stops in the home position to allow the CCD camera to capture an image of the laser spot. Communication protocols implemented in Labview [17] enable the robot controller and CCD camera to work together autonomously. Thermal images of the temperature distribution in the link are taken at the beginning and end of the run.

IV. Analytical analysis

An analytical transient heat flow model is developed to correspond to the stationary case. The analytical analysis is performed to obtain the total longitudinal deformation of the heated slender link. For one-dimensional transient heat flow the change in temperature T at any time τ for location x is [18]:

$$\frac{dT}{dx} = \frac{|T_i - T_o|}{\sqrt{\pi \alpha_d \tau}} e^{-x^2/4\alpha_d \tau}. \quad (1)$$

Thermal diffusivity, α_d, is:

$$\alpha_d = \frac{k}{\rho c},$$

where ρ is the density, k and c are the thermal conductivity and specific heat of the material respectively. At any time τ Equation (1) may be rewritten as:

$$dT = f(x)\, dx. \quad (2)$$

The total longitudinal deformation of the link between the shaft centre and the laser diode centre is of interest at the onset of steady state. When no motion is involved the effects of convection are negligible.

In the absence of restraint, any small element of the link will deform according to:

$$dl = l\alpha\, dT, \quad (3)$$

where l is the nominal length (m), T is the temperature (K), and α is the linear coefficient of thermal expansion (K^{-1}). Combining this result with Equation (2) yields:

$$\Delta L = \alpha L |Ti - To| \ \mathrm{erf}\left(\sqrt{\frac{\rho \mathrm{c}}{\mathrm{k}\tau}}\mathrm{L}\right). \quad (4)$$

The result is an analytic expression for the change in length of the link at any time τ for a change in temperature applied at the location of the shaft. Material properties for the 6061 Al link are listed in Table I.

V. Numerical analysis

ABAQUS [19] is used to perform a coupled thermal-mechanical FEA incorporating transient thermal effects, for the case of the moving link. It is assumed that mechanical effects (e.g. inertia) can be neglected, however convective heat transfer introduced by the motion of the link is included. This analysis provides an understanding of the thermal-mechanical environment of the moving case.

The finite element model uses 8-node trilinear (displacement and temperature) hexahedral elements as shown in Figure 6. The link is modelled with 23 elements along its length, 4 elements across the width and 1 through-thickness element. A representative portion of the hollow drive shaft at the proximal end of the link is modelled with 7 elements along its length and 8 elements around its circumference. The laser diode located at the distal end of the link has 10 elements along its length and 12 elements in the cross section.

Several mesh configurations and thermal convergence criteria were considered. Those presented here, provided good results in an acceptable run time.

A. Material properties

The material properties used in the FEA are summarized in Table I. The link is 6061 Al. The shaft is assumed to be 430 stainless steel. The laser diode is assumed to be ABS plastic. All properties are selected for the expected temperature range of 20°C to 100°C.

B. Thermal boundary conditions

- The initial temperature of the model is prescribed to the ambient temperature of 22°C.
- The motor shaft is heated directly using a heating pad. Accordingly a surface temperature condition of 42°C is applied.
- The convection heat transfer coefficient associated with the motion of the link is $7.75 \frac{W}{m^2\, K}$. Convection is permitted for all free surfaces of the link.
- The duration of the analysis is 1 hour. The maximum allowable temperature change for each of the 64 time increments is 1°C.

C. Mechanical boundary conditions

- The average linear velocity of the link is only 0.5 $\frac{m}{s}$, therefore it is assumed that dynamic mechanical effects such as inertia can be neglected.
- One face of the motor shaft, at the proximal end, is fixed.

VI. Discussion and results

Results from the stationary and moving cases are presented with temperature distributions and temperature-induced deformation. The results from the stationary case indicate that there is a potential to incorporate a simple algorithm to compensate for temperature-induced deformation in the warm-up cycle of the mechanical system.

A. Stationary case: discussion and results

The temperature distribution of the link is obtained from the infrared camera, see Figure 2 for example. The heating pad, the glowing patch on the left hand side, remains at high temperature to keep the temperature of the output shaft constant at approximately 36°C.

The temperature distribution and longitudinal deformation are plotted over the period of 1 hour for the stationary case in Figure 3. Using 3 time constants (define as time it takes to reach $(e-1)/e$ of the steady state value), it can be seen that steady state occurs at approximately 2250 s.

TABLE I. Material properties

Material Property	Symbol	6061 Al [20]	430 SS [20]	ABS [21]
Thermal conductivity ($\frac{W}{m\,K}$)	k	167	26.1	0.27
Density ($\frac{kg}{m^3}$)	ρ	2713	7800	1180
Young's modulus (Pa)	E	7×10^{10}	20×10^{10}	0.23×10^{10}
Poisson's ratio	ν	0.33	0.285	0.3
Linear coefficient of thermal expansion (K^{-1})	α	$23.6 \times 10^{-}6$	$10.25 \times 10^{-}6$	53×10^{-6}
Specific heat ($\frac{J}{kg\,K}$)	c	892	460	1424
Emissivity	ϵ	0.95	0.85	0.91

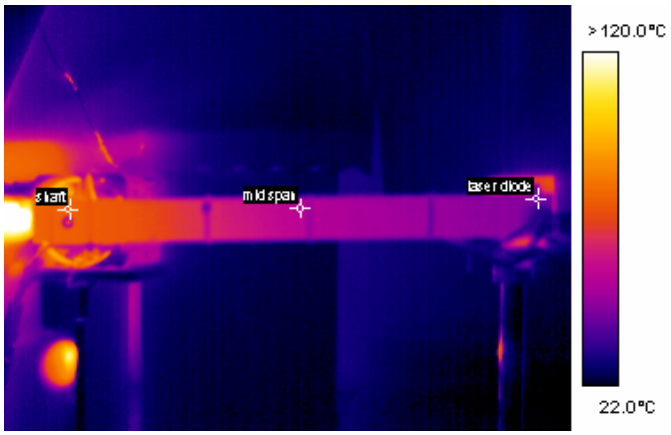

Fig. 2. Temperature distribution at steady state of the stationary case (shown for illustrative purposes only and not for temperature data extraction)

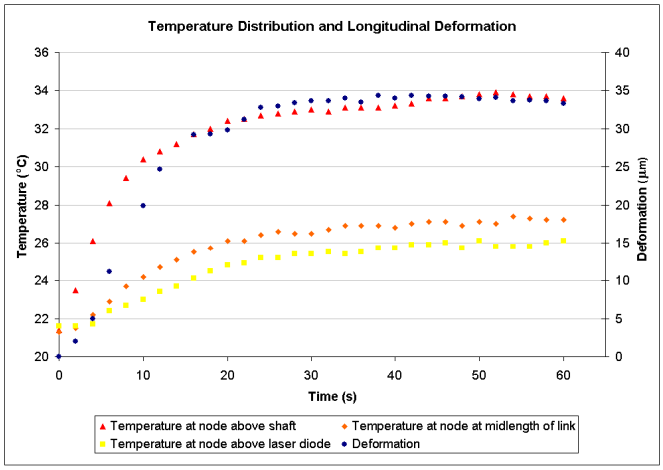

Fig. 3. Temperature distribution and longitudinal deformation in the stationary case

Using Equation (4), the initial and final temperatures of 22°C and 36°C respectively and the material properties listed in Table I, the longitudinal deformation in the stationary case can be obtained. The predicted and experimental results are shown in Table II and are in good agreement.

The agreement between the predicted temperature-induced deformation and the experimentally determined deformation suggests that it may be possible to develop a simple industrial predictive control algorithm for the stationary case. Given some knowledge of motor efficiencies, Equation (4) could be used to predict the temperature-induced deformation in each of the links. The nominal robot dimensions could be adjusted to compensate for the induced end effector error. The stationary case is, however, an over-simplification of virtually all robot workcell environments. Ultimately, the robot controller will require a complex algorithm to incorporate multiple heat sources, their effects and the effects of convection. Such an algorithm may contribute to the reduction of warm-up cycle times.

TABLE II. Analytical and experimental longitudinal deformation of stationary case

	Deformation (μm)
Experimental	34.3
Analytical	33.2
% Difference	3.4

B. Moving case: discussion and results

The steady state temperature distribution for the link as recorded during the experiment for the moving case, is shown in Figure 4. The temperature immediately above the laser diode is 28.2°C and the temperature immediately above the motor shaft is 36.6°C. Note that the temperature of the laser diode, which has a low thermal conductivity, remains at room temperature throughout the experiment, as

expected.

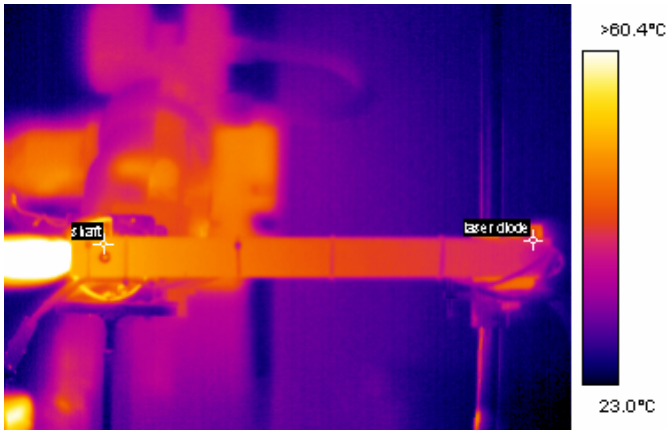

Fig. 4. Temperature distribution at steady state of the moving case (shown for illustrative purposes only and not for temperature data extraction)

Figure 5 shows the temperature history predicted by the transient FEA for the nodes immediately above the laser diode (27.4°C) and the node immediately above the motor shaft (36.0°C). The experimental steady state results are superimposed on Figure 5. Clearly, there is excellent agreement between the FEA and experimental results at steady state. The node above the motor shaft reaches steady state sooner than that of the one above the laser diode.

A fringe plot of the steady state thermal distribution predicted by the FEA is shown in Figure 6. As expected, the temperature changes smoothly over the length of the link, as a function of distance from the motor shaft. Steady state occurs at approximately 1800 s for the node immediately above the laser diode.

Coupled thermal-mechanical effects are of particular interest. The longitudinal deformation predicted at steady state by the FEA, is illustrated in Figure 7.

Figure 8 shows the experimentally measured longitudinal deformation of the point immediately above the laser diode as compared to that of the corresponding node, as predicted by the FEA. Both Figure 8 and Table III show that the FEA generally over predicts the temperature-induced deformation. Some of the difference can be attributed to relative positions of the two locations. However, at steady state the difference is about 3.5%.

The results suggest that the steady state temperature-induced deformation in the moving case can be predicted with similar error to that of the stationary case. Further study of boundary conditions and material properties is required to determine the usefulness of this result. There is no intention to implement the FEA model in the robot controller. However, the convection coefficient could be incorporated in the analytical analysis; e.g., Equation (1). This work will be the subject of further study in the development of an industrial predictive control algorithm.

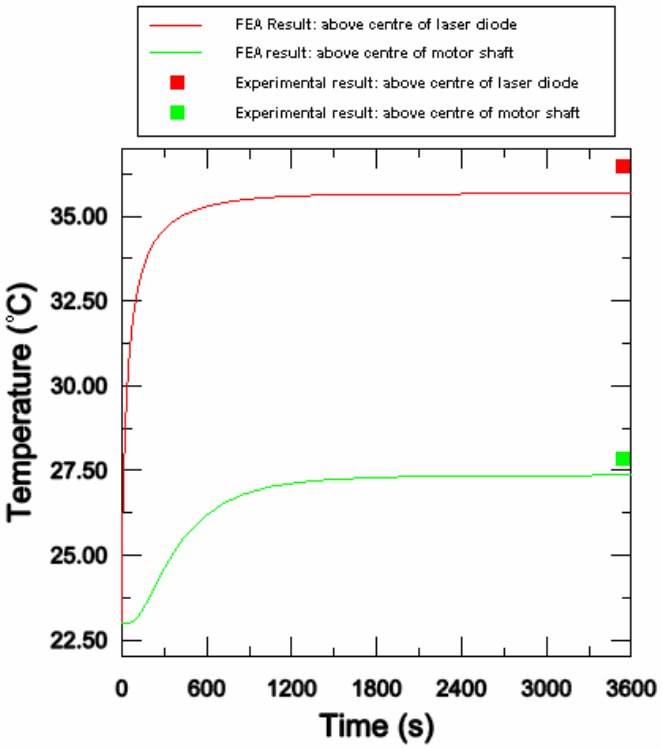

Fig. 5. Temperature of two node locations over the period of 3600 s for the moving case

TABLE III. Numerical and experimental longitudinal deformation of the moving case

	Deformation (μm)
Experimental	45.2
Numerical	46.8
% Difference	3.5

VII. Conclusions

The stationary case shows good agreement in the temperature distributions and temperature-induced deformations of the experimental and analytical results. Similarly, in the moving case, there is good agreement shown between the experimental and numerical results.

The potential for the development of a simple predictive control algorithm to compensate for temperature-induced deformation, and reducing or eliminating warm-up cycle times in industrial robots has been introduced.

References

[1] Poonyapak P. and Hayes M. Towards a predictive model for temperature-induced deformation of an industrial robot. In *Proc. EuCoMeS, the first European Conference on Mechanism Science*, on CD, Obergurgl, Austria, February 2006.

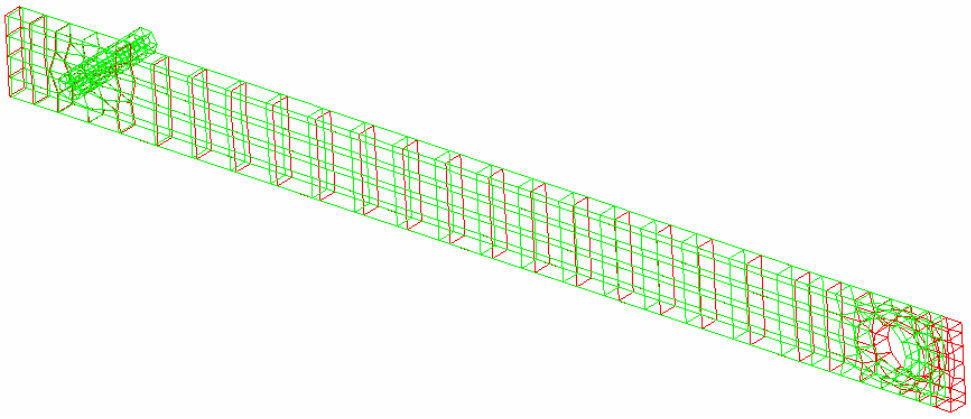

Fig. 7. Longitudinal deformation ($\times 100$) superimposed on undeformed link at steady state for the moving case

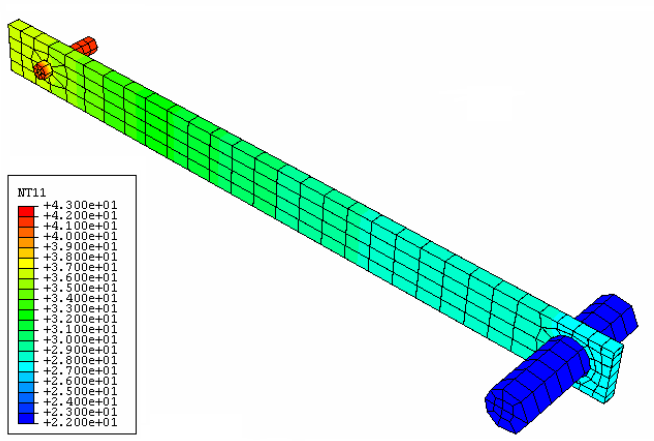

Fig. 6. Temperature distribution in the moving case

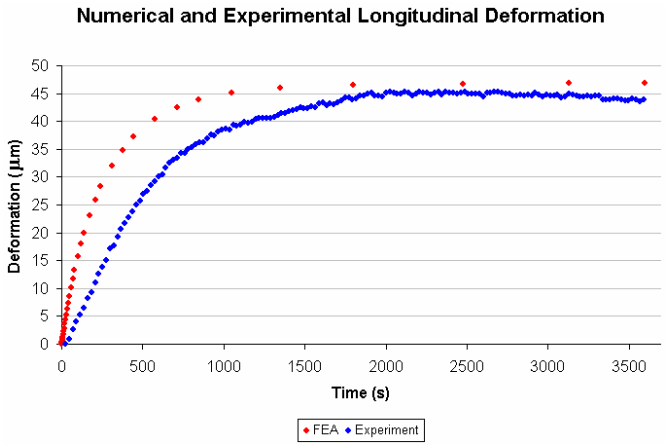

Fig. 8. Longitudinal deformation of numerical and experimental results immediately above the laser diode in the moving case

[2] Großmann K., Wunderlich B. and Szatmari S. Progress in accuracy and calibration of parallel kinematics. In *Proc. Parallel Kinematic Machines in Research and Practise: the 4th Chemnitz Parallel Kinematics Seminar*, pages 49-68, Chemnitz, Germany, 2004.

[3] Hayati S. Robot arm geometric link parameter estimation. In *Proc. 22nd IEEE Conf. on Decision and Control*, pages 1477-1483, San Antonio, 1983.

[4] An C., Atkeson C. and Hollerbach J. *Model-based control of a robot manipulator*. MIT Press, Cambridge, 1988.

[5] Sklar M. Geometric calibration of industrial manipulators by Circle Point Analysis. In *Proc. 2nd Conf. on Recent Advances in Robotics*, Boca Raton, FL, pages 178-202, 1989.

[6] Bennett D. and Hollerbach J. Autonomous calibration of single-loop closed kinematic chains formed by Manipulators with Passive Endpoint Constraints. *IEEE Trans. Rob. & Autom.*, 7:597-606, 1991.

[7] Mooring B., Roth Z. and Driels M. *Fundamentals of manipulator calibration*. John Wiley and Sons, Inc., New York, 1991.

[8] Vincze M., Prenniger J. and Gander H. A laser tracking system to measure position and orientation of robot end effectors Under Motion. *International Journal of Robotics Research*, 13(4):305-314, August, 1994.

[9] Wampler C., Hollerbach J. and Arai T. An implicit loop method for kinematic calibration and its application to closed-chain mechanisms. *IEEE Trans. Rob. & Autom.*, 11(5):710-724, 1995.

[10] Zhuang H. and Roth Z. *Camera-aided robot calibration*. CRC Press, Boca Raton, FL, 1996.

[11] Gong C., Yuan J. and Ni J. A self-calibration method for robotic measurement System. *ASME Journal of Manufacturing Science and Engineering*, 2000.

[12] Hollerbach J. and Wampler C. The calibration index and taxonomy for robot kinematic calibration methods. *International Journal of Robotics Research*, 15:705-712, 1996.

[13] Fratpietro A. and Hayes M. Relative measurement for kinematic calibration using digital image processing. In *Proc. CSME Forum 2004*, University of Western Ontario, London, ON, June 2004.

[14] Simpson N. and Hayes M. Simulation of kinematic calibration procedure that employs the relative measurement concept. In *Proc. CSME Forum 2004*, University of Western Ontario, London, ON, June 2004.

[15] FLIR Systems *Thermovision^{TM} A40M operation's manual*. FLIR Systems, Danderyd, Sweden, October 2004.

[16] Jain R., Kasturi R and Schunck B. *Machine vision* McGraw-Hill Inc., New York, 1995

[17] National Instrument Corporation *Labview^{TM} version 6.1*. National Instrument Corporation, Austin, TX, 2001.

[18] Holman J. *Heat transfer, ninth edition.*. McGraw-Hill Inc., New York, 2002.

[19] ABAQUS, Inc. *ABAQUS/CAE version 6.4.1*. ABAQUS, Inc., Providence, RI, 2003.

[20] Boyer H. and Gall T. *Metals handbook: desk edition*. American Society for Metals, 1985.

[21] Dostal Cyril A. *Engineered materials handbook volume 2: engineering plastic*. American Society for Metals, November 1988.